Anais X SBSR, Foz do Iguaçu, 21-26 abril 2001, INPE, p. 839-846, Sessão Especial - Workshops

Oceanic and Atmospheric Anomalies of Tropical Instability Waves

Paulo S. Polito[1], John P. Ryan[2], W. Timothy Liu[3] and Francisco P. Chavez[2]

Abstract. Tropical instability waves (TIWs) are detected in remotely-sensed sea surface height (SSH), temperature (SST), and wind records of the eastern equatorial Pacific. The highest correlations between TIW geophysical anomalies are observed at 3.5°N. The 71% correlation and 90° phase lag between SSH and SST indicate that TIW SST anomalies are mostly due to advection of the meridional temperature gradient by TIW currents. Meridional (zonal) wind anomalies are significantly correlated and have a 90° (−90°) phase lag with SSH. Ekman pumping (EkP) anomalies are well correlated with both SSH and SST. The difference between wind measurements from TAO moorings and scatterometers is phase-locked with TIW SST oscillations. These evidences support that in the spectral band of TIWs NSCAT and QuikSCAT wind vectors are biased by surface currents. However, the scatterometer stress and its derivatives are unbiased because they depend only on the surface roughness.

Introduction

Equatorial Pacific TIWs have been observed and modeled for more than two decades (*Legeckis* [1977]; *Cox* [1980]; *Halpern et al.* [1988]; *Yu et al.* [1995]; *Qiao and Weisberg* [1998]). TIWs are Rossby or Rossby-gravity waves whose phase always propagates westward and whose group velocity can be either westward or eastward. The waves are generated by barotropic instability and are seasonally and interannually modulated by variations in the system of currents that sustains them.

TIW horizontal phase propagation is mainly zonal with phase speeds (c_p), wavelengths (λ) and periods (P) on the order of -35 km day^{-1}, 1000 km and 30 days. These attributes are based on observational and theoretical results that can vary by more than a factor of two (*Qiao and Weisberg* [1995]), depending on latitude, instrumentation, and time, among other factors.

[1]Instituto Nacional de Pesquisas Espaciais, São José dos Campos, São Paulo, Brazil

[2]Monterey Bay Aquarium Research Institute, Moss Landing, California

[3]Jet Propulsion Laboratory,California Institute of Technology, Pasadena, California

Theory

We present basic theory for phase and scaling arguments essential to interpretation of anomaly relationships.

TIWs are evident as westward propagating anomalies in SSH (η) and SST (SST$'$). η are mostly caused by variations in the density of the water column, dominated by temperature (thermosteric) fluctuations:

$$\eta = \alpha \int_h^0 T(z)\, dz, \tag{1}$$

where α is the thermal expansion coefficient, $T(z)$ the temperature anomaly profile and h a depth below the main thermocline. In Equation 1, a 1°C anomaly extending to 300 m results in a η of 0.1 m. If the temperature anomaly extends to depth h, η and SST$'$ should be in phase.

Strong meridional current fluctuations are associated with TIWs. Owing to equatorial upwelling, the poleward temperature gradient is positive and relatively strong where TIWs develop. SST$'$ due to advection of the meridional SST gradient ($\frac{\partial SST}{\partial y}$) by a meridional geostrophic current anomaly (v_o') acting for a period P are approximately:

$$SST' = v_o' \frac{\partial SST}{\partial y} P, \text{ with } v_o' = \frac{g}{f}\frac{\partial \eta}{\partial x}, \tag{2}$$

where g is gravity, f the Coriolis parameter and x the zonal dimension. Heat and mass exchange are neglected. In Equation 2, a 0.5 m s^{-1} v_o' acting for 15 days in the presence of a meridional SST gradient of 2×10^{-6} °C m^{-1} results in SST$'$ of 1.5 °C. If forced by TIW meridional currents, SST$'$ should lag η by 90°.

Although Ekman pumping does not cause TIWs, we present theory and scaling because TIW-like patterns are observed in the wind stress curl field. EkP anomalies (EkP$'$) cause density fluctuations in the Ekman layer, and thus influence η. The vertical velocity at the base of the Ekman layer is given by the EkP equation, and the vertical velocity of the surface ($\frac{\partial \eta}{\partial t}$) induced by wind forcing is given by EkP$'$ scaled by the stratification:

$$\frac{\partial \eta}{\partial t} = -\frac{\nabla_k \times \vec{\tau}}{\Delta \rho f}, \tag{3}$$

where $\Delta\rho$ is the density difference between the layers above and below the base of the Ekman layer, and $\nabla_k \times \vec{\tau}$ is the vertical component of the wind stress curl. The wind stress curl is in phase with the vertical velocity and thus at 90° with its integral, η. With thermal stratification, Ekman upwelling can result in SST cooling. In Equation 3, considering only the spectral band associated with TIWs, a wind anomaly of 3 m s^{-1} over $\frac{1}{2}\lambda$ of a TIW would force vertical displacement of isotherms of $\sim$ 10 m in 15 days. In this region, the thermal stratification is such that a 10 m displacement would result in SST$'$ of $\sim$ 0.5 °C.

Data Sets and Methods

To examine the relationship between TIW geophysical anomalies we used WOCE TOPEX/POSEIDON SSH data, daily 9-km AVHRR Pathfinder SST, and daily NASA Scatterometer (NSCAT) 0.5° Level 3 winds. The period examined coincides with the NSCAT period, September 1996 through May 1997. The spatial domain extends between the date line and 100° W, 10.5°S and 10.5°N. The SSH data were acquired bin-averaged at 0.5° × 0.5° × 10.0 days. Daily SST and wind fields were averaged into 7-day, 2° latitude bins at the zonal resolution of the data. All data sets were interpolated *via* bicubic gridding to a common 0.5° × 7-day zonal-temporal grid.

For computing EkP, wind stress was calculated according to *Large and Pond* [1981]. This parameterization is not ideal for the equatorial region, particularly at low wind conditions. However, because the drag coefficient is a simple function of wind speed, any TIW patterns found in the stress and its derivatives are a direct result of wind anomalies. Considering that the magnitude of the stress is only used for scaling purposes and the measurement of low wind speed always has large inherent errors, the choice of a simple drag coefficient is justified.

Anomalies were computed for all variables by removing the temporal mean. All anomaly time series were then band-pass filtered using the same series of 2D (zonal-temporal) finite impulse response filters (*Polito and Cornillon* [1997]). The strength of the TIW signal in each variable is estimated by the amount of total variance explained by the filtered signal (σ). For each pair of variables the zonal-temporal cross-correlation matrix was calculated. A sinusoidal surface was least-squares fit to the correlation to obtain the maximum correlation (C_{max}) within one λ and P of the origin, and the average phase difference ($\Delta\Phi$). Because of the coarse resolution of the data in relation to the wave period, $\Delta\Phi$ are estimated only to the nearest 90° increment.

To compare buoy and scatterometer winds in the TIW region we examined all buoys East of 160° W for both the 1996-1997 TIW season observed by NSCAT and the 1999-2000 TIW season observed by QuikSCAT (0.25° Level 3).

Results and Discussion

TIW signals are most clearly evident in the NSCAT record in the 2° latitude bands centered at 1.5°N and 3.5°N, between 160°W and 120°W and October/96 through January/97. Outside this band the fractional variance of the filtered SST′ signal is <10%, and its correlation with η is <50%. Because the amount of variance explained by the filtered signals was greatest at 3.5°N, we present results from this latitude band (Figure 1). The TIW signals are evident in zonal-temporal plots as diagonally-oriented bands of positive and negative anomalies whose orientation indicates westward phase propagation (dashed line). TIW anomalies are evident in the unfiltered data, together with strong, large scale signals that are removed by the 2D band-pass filter. From filtered anomalies, the estimates of $c_p \sim 37$ km day^{-1}, $P \sim 30$ days, and $\lambda \sim 1100$ km are in agreement with previous estimates for TIWs (*Qiao and Weisberg* [1995]). Anomaly statistics are summarized in Table 1.

Table 1. Summary of the results. Positive $\Delta\Phi$ indicates that the the first parameter leads the second.

parameter	σ	parameters	$\Delta\Phi$	C_{max}
η	30%	η,SST′	90°	71%
SST′	30%	η,v'	90°	68%
u'	21%	η,u'	−90°	66%
v'	28%	η,EkP′	0°	60%
EkP′	40%	SST′,v'	0°	62%
		SST′,u'	−180°	78%
		SST′,EkP′	−90°	61%

The high correlation and quadrature of phase between η and SST′ (Table 1) have two important interpretations. First, they indicate that TIW SST′ are not in phase with upper layer thermosteric anomalies (Equation 1). Second, they suggest that advection of

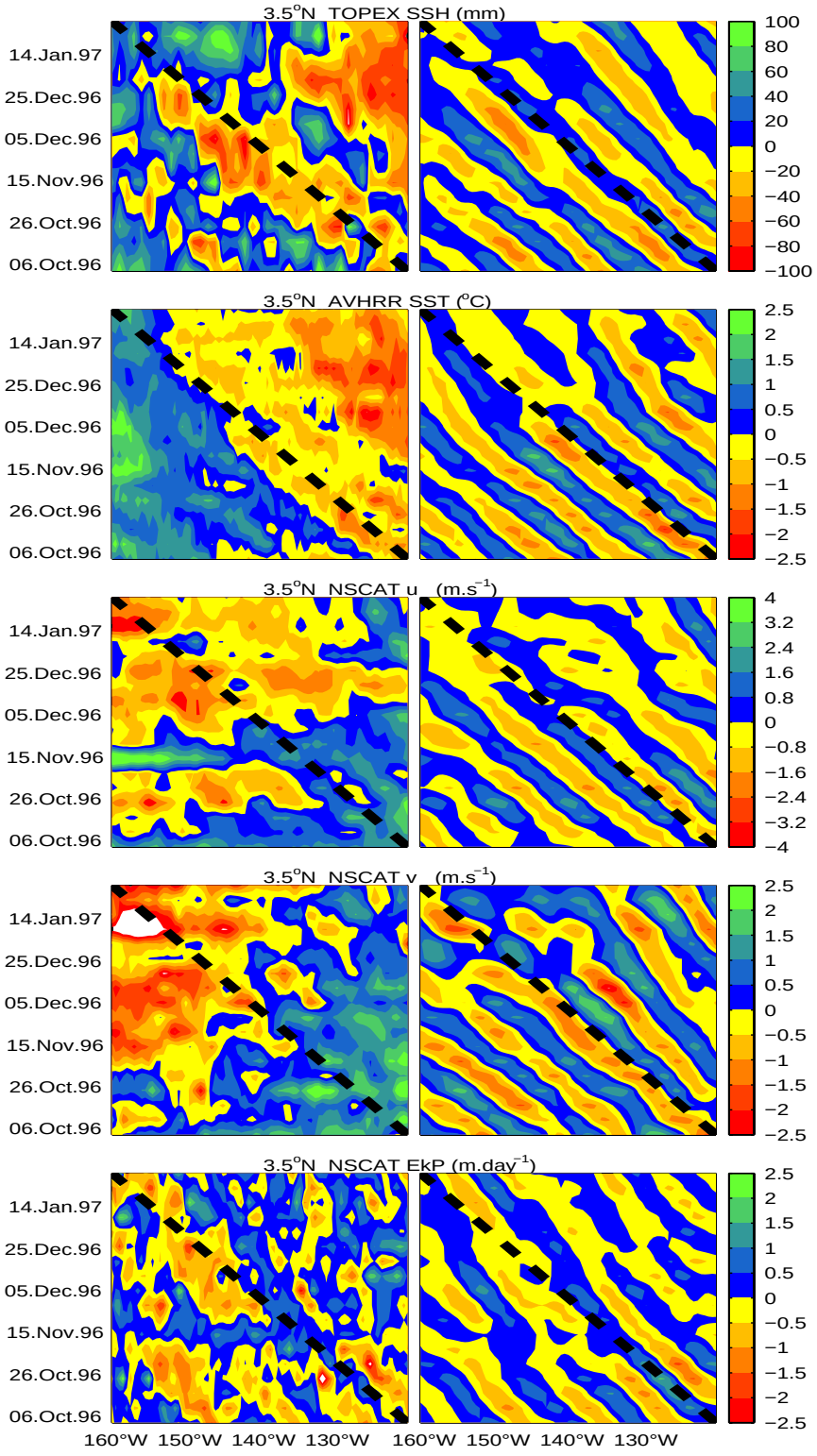

Figure 1. Zonal-temporal diagrams of unfiltered (left) and filtered (right) η, SST$'$, v' and EkP$'$.

the meridional temperature gradient by TIW geostrophic currents causes SST′ (Equation 2). Northward currents associated with the positive zonal η slopes of TIWs advect cold SST northward, while southward currents associated with negative zonal η slopes advect warm SST southward. This interpretation is consistent with high resolution mapping of circulation and SST over a TIW (*Flament et al.* [1996]).

Zonal and meridional wind anomalies (u', v') also show a strong, clear TIW signal (Figure 1). v' are highly correlated with both η and SST′ and are in quadrature with η (Table 1) thus in opposition of phase with TIW geostrophic surface currents. A plausible hypothesis for a relationship between η and v' in this spectral band is that TIW currents affect scatterometer wind retrievals. As demonstrated by *Liu and Large* [1981], spacebased scatterometer measurement is more closely related to surface stress than wind. The algorithm relating equivalent neutral wind to NSCAT observations was derived on the assumption that ocean currents are negligible compared with wind. We propose that scatterometer winds over TIWs are biased by enhanced surface roughness caused by surface currents. This hypothesis is supported by comparison of buoy and scatterometer winds in the TIW region (Figures 2 and 3). The difference between the QuikSCAT and TAO mooring winds is phase–locked with the TIW SST′. The relationship apparent in Figures 2 and 3 breaks down at the end of the TIW season in January 2000. The same results are evident in the NSCAT record, albeit less clearly.

The TIW signal in EkP′(Figure 1) is strongly correlated with both η and SST′ (Table 1). η and EkP′ are in phase. The expected phase lag for EkP′ forcing η is 90° (Equation 3). Based on correlation and phase relationships, we argue that TIW SST′ are predominantly forced by meridional current anomalies. Although EkP′ can force SST′, this relationship is not supported. First, EkP′ leads SST′ by 90° (Table 1). For EkP′ forcing of SST′, SST′ should lead EkP′ by 90°. Second, considering the relatively weak thermal stratification of the upper 10 m, SST cooling by Ekman upwelling would be ~ 0.5 °C, significantly less than the observed SST′ (Figure 1).

The EkP′ are consistent with enhanced meridional wind stress gradients within a latitude band (Figure 1). East (west) of a positive η, meridional winds would have a northward (southward) anomaly. This would appear as a wind stress curl anomaly in phase with η, as observed. EkP′ due to surface ocean currents are analogous to inverted Ekman pumping resulting from bottom friction.It is important to distinguish between the influence of ocean currents on scatterometer wind velocity estimates and EkP derived from scatterometer winds. The results presented here support that wind velocity bias is caused by scatterometer detection of enhanced stress at the air–sea interface due to ocean currents. Although wind velocities are biased, the enhanced stress causing the bias is real, and thus so are the EkP′.

Surface stress enhancement by strong TIW ocean currents is distinct from the air–sea coupling described by *Liu et al.* [2000] and *Chelton et al.* [2000] in which SST anomalies in the TIW region influence surface wind speed through modification of boundary layer stability. Both of these air–sea coupling phenomena have important biogeochemical implications. Convergence and divergence that develop with TIWs affect biological distributions and processes (*Yoder et al.* [1994]; *Flament et al.* [1996]; *Chavez et al.* [1999]). TIW EkP′ may force

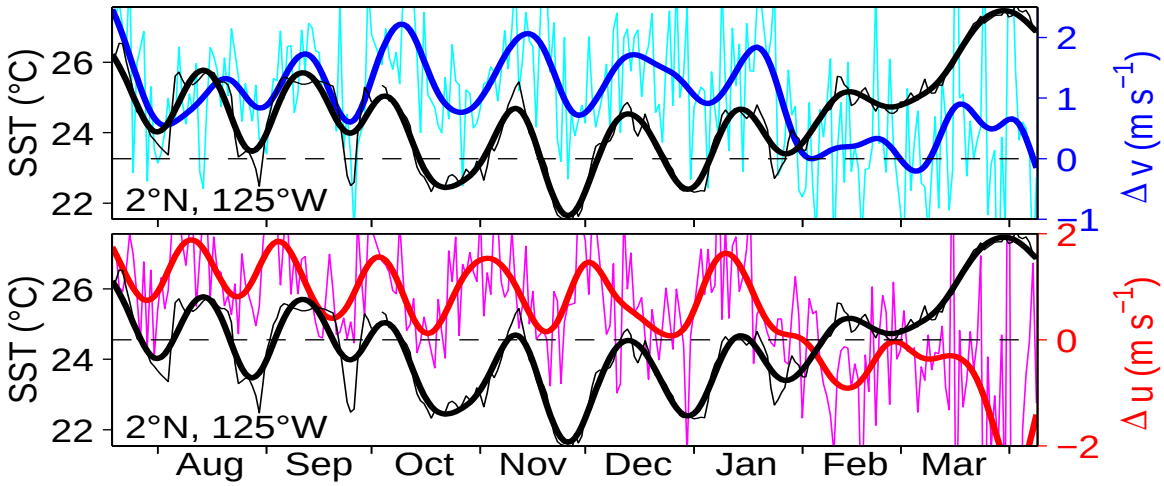

Figure 2. Difference between Quikscat and TAO buoy wind components, from July 1999 to April 2000, compared to TAO buoy SST (black). Thick curves show 20-day low pass filtered data.

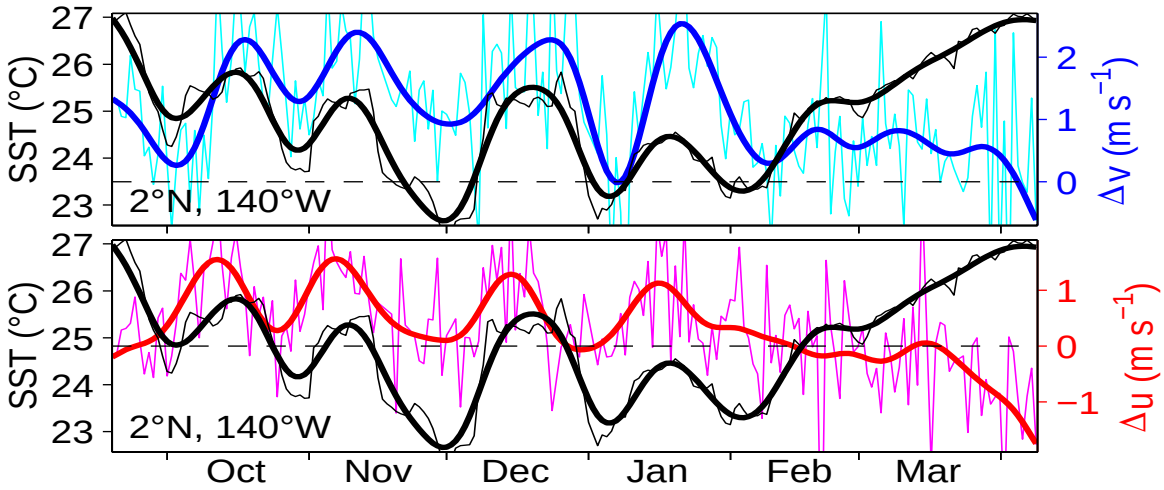

Figure 3. As in Figure 2.

variation in vertical nutrient flux in this biogeochemically important upwelling system. Thus we state not only caution regarding bias in scatterometer wind velocities, but also motivation to use scatterometer data to understand dynamical and biological effects of air–sea stress anomalies.

Acknowledgments. P. Polito was jointly supported by the Physical Oceanography and Earth Observing System Interdisciplinary Sciences Programs of NASA. J. Ryan was supported by the David and Lucile Packard Foundation. We thank the Physical Oceanography Distributed Active Archive Center at NASA Jet Propulsion Laboratory for provision of all satellite data sets used in this study. Acquisition of the NSCAT Level 3 data was facilitated by the Distributed Oceanographic Data System (http://www.unidata.ucar.edu/packages/dods).

References

Chavez, F. P., P. G. Strutton, G. E. Friedrich, R. A. Feely, G. Feldman, D. Folay and M. J. McPhaden, Biological and chemical response of the equatorial Pacific Ocean to the 1997-98 El Niño, *Science286*, 2126-2131, 1999.

Chelton, D. B., F. J. Wentz, C. L. Gentemann, R. A. de Szoeke and M. G. Schlax, Satellite microwave SST observation of transequatorial tropical instability waves, *Geophys. Res. Lett., 27*, 1239–1242, 2000.

Cox, M. D., Generation and propagation of 30-day waves in a numerical model of the Pacific, *J. Phys. Oceanogr., 10*, 1168–1186, 1980.

Flament, P. J., S. C. Kennan, R. A. Knox, P. P. Niiler and R. L. Bernstein, The three-dimensional structure of an upper ocean vortex in the tropical Pacific Ocean, *Nature*, *383*, 610–613, 1996.

Halpern, D., R. A. Knox, and D. S. Luther, Observations of 20-day period meridional current oscillations in the upper ocean along the pacific equator, *J. Phys. Oceanogr., 18*, 1514–1534, 1988.

Large, W. G. and S. Pond, Open ocean momentum measurements in moderate to strong winds. *J. Phys. Oceanogr., 11*, 324–336, 1981.

Legeckis, R., Long waves in the eastern equatorial Pacific ocean: a view from a geostationary sattelite, *Science*, *197*, 1179–1181, 1977.

Liu, W.T. and W.G. Large, Determination of surface stress by Seasat-SASS: A case study with JASIN Data. *J. Phys. Oceanogr.*, , *11* , 1603-1611, 1981.

Liu, W. T., X. Xie, P. S. Polito, S.–P. Xie and H. Hashizume, Atmospheric manifestation of tropical instability wave observed by QuikSCAT and Tropical Rain Measuring Mission. *Geophys. Res. Lett.*, , *27*, 2545–2548, 2000.

Polito, P. S., and P. Cornillon, Long baroclinic Rossby waves detected by TOPEX/POSEIDON, *J. Geophys. Res., 102*, 3215–3235, 1997.

Qiao, L., and R. H. Weisberg, Tropical instability wave kinematics: observations from the tropical instability wave experiment (TIWE), *J. Geophys. Res., 100*, 8677–8693, 1995.

Qiao, L., and R. H. Weisberg, Tropical instability wave energetics: observations from the tropical instability wave experiment, *J. Phys. Oceanogr., 28*, 345–360, 1998.

Yoder, J. A., S. G. Ackleson, R. T. Barber, P. Flament and W. M. Balch, *Nature*, *371*, 689–692, 1994.

Yu, Z., J. P. McCreary, and J. A. Proehl, Energetics of tropical instability waves, *J. Phys. Oceanogr., 25*, 2997–3007, 1995.

P. S. Polito, Instituto Nacional de Pesquisas Espaciais, Divisão de Sensoriamento Remoto, Av. dos Astronautas,1.758, São José dos Campos, SP, Brazil, CEP: 12227-010 (e-mail: polito@pacific.jpl.nasa.gov)

W. T. Liu, Jet Propulsion Laboratory, California Institute of Technology, 4800 Oak Grove Dr., MS 300-323, Pasadena CA 91109. (e-mail: liu@pacific.jpl.nasa.gov)

J. P. Ryan and F. P. Chavez Monterey Bay

Aquarium Research Institute, 7700 Sandholdt Road,
Moss Landing, CA 95039. (e-mail: ryjo@mbari.org;
chfr@mbari.org)